Targeted delivery of adamantylated peptidoglycan immunomodulators in lipid nanocarriers: NMR shows that cargo fragments are available on the surface

Rosana Ribić, Mateja Manček-Keber, Fernando Chain, Davy Sinnaeve, José C Martins, Roman Jerala, Srđanka Tomić, Krisztina Fehér

Targeted delivery of adamantylated peptidoglycan immunomodulators in lipid nanocarriers: NMR shows that cargo fragments are available on the surface

Rosana Ribić,#[a] Mateja Manček-Keber,#[b] Fernando Chain,[c] Davy Sinnaeve,[c,d] José C. Martins,[c] Roman Jerala,[b] Tomić Srđanka,[e] and Krisztina Fehér[c,f,g]*

[a] University Center Varaždin, University North, Jurja Križanića 31b, HR-42 000, Varaždin, Croatia

[b] Department of Synthetic Biology and Immunology, National Institute of Chemistry, Hajdrihova 19, POBox 660, SI-1001 Ljubljana, Slovenia

[c] Department of Organic and Macromolecular Chemistry, Ghent University, Campus Sterre S4, Krijgslaan 281, 9000, Ghent, Belgium

[d] CNRS, Unité de Glycobiologie structurale et fonctionnelle UMR 8576, 50, Avenue de Halley, Campus CNRS de la Haute Borne, F-59658 Villeneuve d'Ascq, France

[e] Department of Chemistry, Faculty of Science, University of Zagreb, Horvatovac 102A, HR-10 000, Zagreb, Croatia

[f] Heidelberg Institute for Theoretical Studies, Schloss-Wolfsbrunnenweg 35, 69118 Heidelberg, Germany

[g] MTA-DE Molecular Recognition and Interaction Research Group, University of Debrecen, Egyetem tér 1, H-4032 Debrecen, Hungary

*Corresponding author Krisztina Fehér, email: feher.krisztina@science.unideb.hu, Tel. +36-52-512900 E-mail: krisztina.feher@h-its.org

Keywords: peptidoglycan, adjuvant, lipid encapsulation, bicelle, NMR spectroscopy

Abbreviations: peptidoglycan (PGN), Pulsed Field Gradient Stimulated Echo (PFGSE), Saturation Transfer Difference (STD), Paramagnetic Relaxation Enhancement (PRE), transferred Nuclear Overhauser Enhancement (transferred NOE), adamantylated glycine (Ada), D-*iso*glutamine (D-iGln), linker residue (Lnk)

Abstract

We present an in-depth investigation of the membrane interactions of peptidoglycan-based immune adjuvants designed for lipid-based delivery systems using NMR spectroscopy. The derivatives contain a cargo peptidoglycan (PGN) dipeptide fragment and an adamantyl group, which serves as an anchor to the lipid bilayer. Furthermore, derivatives with a mannose group that can actively target cell surface receptors on immune cells are also studied. We showed that the targeting mannose group and the cargo PGN fragment are both available on the lipid bilayer surface, thereby enabling interactions with cognate receptors. We found that the non-mannosylated compounds are incorporated stronger into the lipid assemblies than the mannosylated ones, but the latter compounds penetrate deeper in the bilayer. This might be explained by stronger electrostatic interactions available for zwitterionic non-mannosylated derivatives as opposed to the compounds, in which the charged N terminus capped by mannose groups. The higher incorporation efficiency of the non-mannosylated compounds correlated with larger relative enhancement in immune stimulation activities upon lipid incorporation compared to the derivatives with the mannose group. The chirality of the adamantyl group also influenced the incorporation efficiency, which in turn correlated with membrane associated conformations that affect possible intermolecular interactions with lipid molecules. These findings will help improving the development of PGN-based immunes adjuvants suitable for delivery in lipid nanoparticles.

Introduction

Development of safe and effective adjuvants in vaccine research is still a challenge[1] as many effective immune modulatory compounds have significant adverse effects, while commonly used safe adjuvants, such as alumn[2], are not very potent. Stimulation of the immune response and modulation of the appropriate type of immunity can be achieved by activation of the innate immune system via activation of Pattern Recognition Receptors (PRRs) expressed on immune cells and other cells. Targeting different PRRs by microbial danger signals, so called Pathogen Associated Molecular Patterns (PAMP), trigger signaling cascades leading to specific proinflammatory responses. Immune adjuvants with various characteristics thus can be obtained by using fragments or analogues of PAMPs[3].

Bacterial cell wall peptidoglycan (PGN) is one of the most important microbial signatures recognized by innate immune receptors. PGN is recognized[4] by intracellular NOD-like receptors NOD1 and NOD2 and secreted peptidoglycan recognition proteins among others. It has been shown that polymeric PGN can stimulate immune defenses even without the presence of an infection, therefore it can act as a very potent adjuvant[5], however, it also has too many side effects to be used in vaccines[6]. Fragments and substances[7] derived from PGN also exhibit weaker adjuvant activities with diminished adverse effects. One of the most widely used PGN fragment is muramyl-dipeptide[8] (MDP) containing the *N*-acetylmuramyl-L-alanyl-D-isoglutamine (L-Ala-D-iGln) motif of PGN, which is the minimal essential unit of PGN. MDP is recognized by NOD2[9], a cytoplasmic receptor of innate immune system, and has weak immune modulatory effect[8] as it is rapidly excreted into the urine and its administration is associated with various adverse side effects.

In order to improve the adjuvant properties of PGN fragments, an appropriate drug delivery system is needed, which can improve metabolic stability and bioavailability, enable reduction of therapeutic doses and thereby reduce adverse effects. The use of lipid nanoparticles as carriers are well-established[10] and have found widespread application in vaccination as many carriers are able to stimulate the immune system and induce both cellular and humoral immune responses[11]. Similarly,

many lipophilic derivatives of MDP were developed to increase loading in lipid carriers[11-12], which increased adjuvant activities and reduced side effects[13].

The PGN derivatives[14] we investigate in this study are designed to be suitable for encapsulation into liposomes. These derivatives contain only a minimal PGN fragment, L-Ala-D-iGln, as a cargo, and an adamantyl group to increase hydrophobicity and to facilitate the anchoring of the PGN fragment cargo to the membrane. Due to the chirality of the adamantyl group, two diastereoisomers were obtained (Scheme 1a and b), which were both shown to be stable, non-pyrogenic, water soluble, non-toxic and displayed an adjuvant effect *in vivo* in mice models[15-16].

Adamantane based drugs are used as antivirals[17-18] as well as in the treatment of Parkinson's[19-20] and Alzheimer's[21-22] disease. They often act at as channel blockers[23-25], but their therapeutic effect was also suggested to be related to nonspecific interactions with membranes[26-27]. Indeed, the hydrophobicity and unique geometry of adamantane is thought to increase membrane permeability and adsorption of drugs and as a result significantly modifies the pharmacological properties of drug molecules. Amantadine (1-aminoadamantane) is one of the oldest and most well-known adamantane containing drugs and its membrane interaction is thought to play a crucial role in its activity[28-30].

We also investigated versions of the adamantylated PGN compounds conjugated to mannose moieties (Scheme 1c and d). Glycosylation with carbohydrates that specifically bind to endogenous lectin receptors on cell surfaces achieve active targeting, which is an important aspect of any drug delivery system as it is more controllable and efficient than passive targeting. Effectiveness of targeting using mannose was shown for mannosylated liposomes, which were found to enhance uptake and activation of dendritic cells and to increase T cell proliferation[31]. In this fashion, antigen presenting cells are targeted, such as macrophages and dendritic cells that express C type lectins (CLR), which can recognize the mannose targeting group. CLR recognition may result in improved internalization and presentation of antigens by Antigen Presenting Cells[32] and may also modulate the immune response via signaling pathways[33]. The former could help increasing uptake of the mannosylated compounds and thus achieve active targeting, while the latter might lead to the modification of the host defense response triggered by the PGN fragment via PRR crosstalk. The adjuvant activity of the

mannosylation in the adamantylated compounds were indeed found to be amplified *in vivo*[14, 16], which might be related to targeting of immune cells.

a) D-Ad_1Tp **DAda – LAla – D*i*Gln**

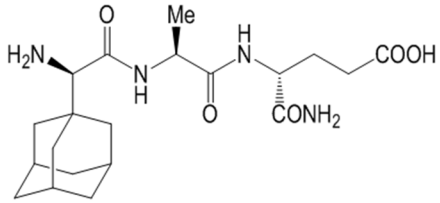

b) L-Ad_1Tp **LAda – LAla – D*i*Gln**

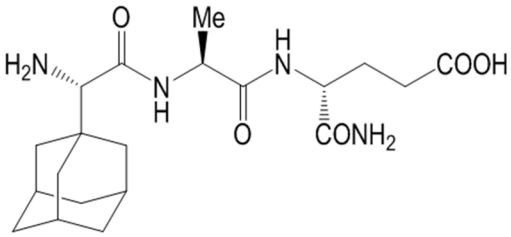

c) Man-D-Ad_1Tp **Man - R-Lnk - DAda – LAla – D*i*Gln**

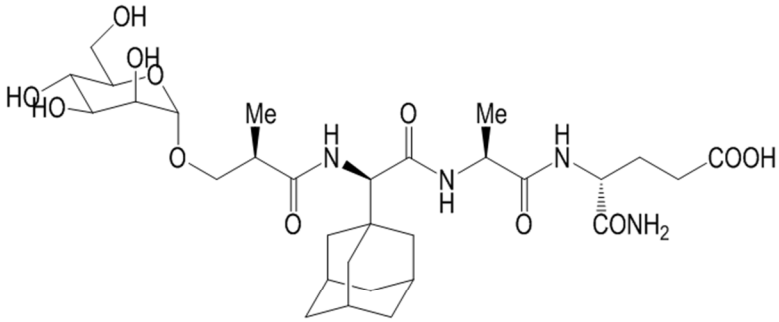

d) Man-L-Ad_1Tp **Man - R-Lnk - LAda – LAla – D*i*Gln**

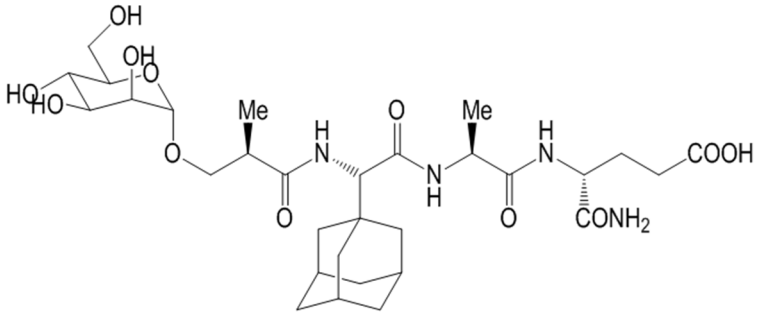

Scheme 1. Chemical structure of the investigated PGN derivatives: ***D-Ad₁Tp***: D-(adamant-1-yl)-Gly-L-Ala-D-*iso*Gln, ***L-Ad₁Tp***: L-(adamant-1-yl)-Gly-L-Ala-D-*iso*Gln, ***Man-D-Ad₁Tp***: (2R)-*N*-[3-(α-D-mannopyranosyloxy)-2-methylpropanoyl]-D-(adamant-1-yl)-Gly-L-Ala-D-isoGln, ***Man-L-Ad₁Tp***: (2R)-*N*-[3-(α-D-mannopyranosyloxy)-2-methylpropanoyl]-L-(adamant-1-yl)-Gly-L-Ala-D-*iso*Gln. * The "Ad_1" notation indicates an adamant-1-yl attachment, the "Tp" notation stands for tripeptide. Ada

stands for adamantylated glycine, D-iGln for D-*iso*glutamine, Lnk for Linker residue including the -CH_2-CH(Me)- fragment.

The PGN derivatives exhibited adjuvant activities *in vivo* in experiments performed in mice model using ovalbumin (OVA) as an antigen[14-15]. Differences regarding the configuration on stereogenic centre of adamantly glycine were observed as D-AdTp showed higher stimulation of anti-OVA IgG antibodies production in comparison to L-AdTp[15]. The best adjuvant activity was observed for the mannosylated derivate Man-D-AdTp[16]. Adjuvant effects of the adamantylated PGN derivatives were also assessed[34] in an *in vitro* assay monitoring cytokine and chemokine production in immortalized mouse bone-marrow derived macrophages. We found that while the PGN compounds do not stimulate macrophages alone, however, L-Ad_1Tp and, in particular, Man-L-Ad_1Tp, were able to enhance the immune responses induced by LPS on macrophages. Moreover, the co-stimulation activity on macrophages was further increased by the incorporation of the compounds into phosphatidylcholine liposomes.

In order to develop improved adjuvant delivery systems for vaccination, understanding of the molecular details governing encapsulation of adjuvants into lipid bilayers and their interactions with the targeted receptors is mandatory. NMR spectroscopy is a powerful technique for investigating the molecular details of membrane interactions of lipid embedded molecules such as detection of interactions, membrane associated structures of solutes, their position and orientation in the membrane as well as determination of entrapment efficiency. The sign dependence[35] of the Nuclear Overhauser Effect (NOE) on the size of the molecule associated to the membrane can reveal the presence of a weak interaction: while non-interacting small molecules are characterized by weak, positive NOEs in their 2D NOESY spectrum, membrane associated molecules show transfer NOEs[36] that are strong and negative. Assignment of the intramolecular NOE cross peaks can reveal the structure of the membrane bound conformation of the molecules, while intermolecular NOEs, if detectable, can pinpoint the interaction with the lipid molecules. Furthermore, Saturation Transfer Difference Spectroscopy[37] (STD) can be used to probe the depth and orientation of the molecule within the lipid bilayer[30] via an epitope mapping procedure[38] identifying the part of the molecule[39] interacting with lipid host. Special

care needs to the taken to address artefacts distorting STD effects arising from differential relaxation times[40]. Solvent accessible fragments of molecules immersed in membranes can be monitored[41] using water soluble paramagnetic probes by inducing Paramagnetic Relaxation Enhancement[42] (PRE) that can be detected by measurement of transverse relaxation times[43] (T_2). Manganese(II) ions[43] induce strong PREs due to five unpaired electrons and long electron relaxation times, but have an isotropic electron g-tensor, thus do not generate pseudocontact shifts. Finally, Diffusion Ordered Spectroscopy[44] (DOSY) provides means to measure the lipid entrapment efficiency of molecules[45] by determining the ratio of free and bound solute in case of fast exchange between the solutes and the bilayer.

In this report, we investigated all four PGN fragment-containing derivatives shown in Scheme 1 using NMR spectroscopy to reveal the molecular details of their interaction with lipid molecules and to establish their lipid encapsulation efficiency. The location and orientation of the derivatives within the bilayer are studied together their membrane associated conformations. This allows assessing the availability of the targeting group and the PGN cargo fragment towards interaction with their corresponding receptors.

Since NMR investigation of large liposomes is not straightforward due to their size and heterogeneity, we used isotropic bicelles[46-47] as model bilayer systems. Here a short-chain phospholipid, used as a detergent, is mixed with long-chain phospholipids, thereby forming disk-like bilayers[48-50] with the rims covered by the detergent-like short-chained phospholipid molecules. Bicelles are considered as good models of lipid assemblies with bilayer structures[51-53]. Specifically, phosphatidylcholine lipids with dimyristoyl and dihexanoyl chains were used as model lipids[54] (DMPC) and detergents (DHPC), respectively. Both DMPC and DHPC carry positively charged choline groups and negatively charged phosphate groups in the head region, which is than bridged by polar glycerol moieties to the fatty acid tails. For the purpose of the NMR characterization we utilized a molar ratio of 0.5 between the detergent and bilayer forming lipids in order to generate isotropically tumbling bicelles.

Experimental and computational methods

Materials Protonated 1,2-dimyristoyl-sn-glycero-3-phosphocholine (DMPC) and 1,2-dihexanoyl-sn-glycero-3-phosphocholine (DHPC) with >99% purity was purchased from Avanti Polar Lipids, Inc. in powder form. Deuterium oxide (D_2O) with a purity >99.9 atom % D was purchased from EurisoTop (France). N-acetyl-glucosamine was purchased from Sigma Aldrich. PGN derivatives were synthesized as previously described[14-15].

NMR spectroscopy The NMR samples contained ca. 20 mg of the PGN derivatives dissolved in 500 µL water containing 10% D_2O. Later an aliquot of the aqueous sample was used for preparing a lipid bicelle sample with ca. 8mM PGN compound concentration in 100mM K phosphate buffer at pH 7.2. 100mM DMPC and 200mM DHPC concentrations were used for making the lipid bicelle solution with a molar ratio of q=0.5 according to described procedures[47]. NMR experiments were performed at 298.3K and 310.2K on a Bruker Avance II NMR spectrometer operating at 700.13MHz equipped with a 5mm TXI-Z probe. The ^{1}H resonances were assigned using standard homonuclear and heteronuclear correlation experiments.

Structure calculation of the membrane-associated state Distance restraints were extracted from a 2D NOESY spectrum measured with 100 ms mixing time at 700.13MHz at room temperature. All transfer NOE cross peaks were manually assigned and integrated by using the CCPNMR software[55]. Signals arising from γ and ε positions of methylene groups in the adamantyl moiety could not be unambiguously assigned, therefore ambiguous restraints were implemented. The signal intensities were converted to distances by calibration against the average of the integrals of all NOE intensities, corresponding to a reference distance of 3.2 Å. For structure calculation, the simulation engine CNS 1.3[56] was employed using a simulated annealing algorithm in torsion angle space with subsequent refinement in explicit water[57]. The CNS force field used for peptides with explicit hydrogens were supplemented with topologies and parameters developed for an amino acid containing adamantyl group in D and L configuration, the linker residue and for D-iGln. An ensemble of structures was generated using an acceptance test selecting structures with no bond length, valence angle and NOE

violations. The obtained structures were aligned along Cα atoms using Discovery Studio Visualizer 3.5[58]. The structures were visualized in PyMOL[59].

Saturation Transfer Difference experiments STD spectra were measured using a pulse sequence with interleaved on- and off-resonance experiments[37]. Saturation of the lipid resonances was performed using a train of selective Gaussian pulses of 49 ms duration and 75 Hz field strength each, separated by a 1 ms delay. The on-resonance frequency used for saturation of the lipid signals was set to 0.74 ppm for the lipid tail (fatty acid chain terminal methyl group of DMPC, 14-Me) and 5.22 ppm for lipid head groups (2'CH of glycerol in DMPC/DHPC). The off-resonance irradiation was applied at −50 ppm outside the area of NMR resonances. The overall saturation time was 6 s and 4096 scans were measured. For the epitope mapping analysis[38], STD signals in the amide region were used, because the aliphatic region of the spectra was dominated by the lipid signals. Control experiments were run using aqueous samples of the derivatives and resulted in signal thus confirming that no glycopeptide resonances were irradiated. The resulting intensities were normalized to reference spectrum intensities with irradiation at -50 ppm and STD amplification factors were obtained. Furthermore, the STD amplification factors were corrected for differences in T_1 relaxation times of the individual ligand protons[40, 60].

Determination of ^1H T_1 relaxation times ^1H T_1 relaxation times were determined in inversion recovery experiments. Water signal was suppressed using excitation sculpting[61]. The inter-scan delay was set to 6 s. The delay during the inversion recovery measurements was varied between 50 ms and 5 s randomly sampled over 16 experiments. The T_1 relaxation time constants were fitted to the obtained data points with the T_1/T_2 Analysis function implemented in TopSpin 3.1.

Paramagnetic Relaxation Enhancement (PRE) experiments Manganese (II) ion was used as a water-soluble paramagnetic relaxation agent, which was added to the samples containing 8mM PGN derivative and 100 mM DMPC and 200 mM DHPC at 0.5 mM, 1 mM and 2 mM concentrations. The effect of the paramagnetic ions was monitored by determination or estimation of T_2 relaxation times. At low paramagnetic ion concentrations, the ^1H T_2 relaxation times were determined in a CPMG experiment using the pulse sequence removing J modulation[62]. The water signal was suppressed using

Excitation Sculpting[61]. The inter-scan delay was set to 6s. The delay in the spin echo was 1.5 ms and the total echo time was varied between 6 ms and 1248 ms randomly sampled over 16 experiments. The T_2 relaxation time constants were fitted to the obtained data points with the T_1/T_2 Analysis function implemented in TopSpin 3.1. For estimation of T_2 relaxation time at higher paramagnetic ion concentrations, linewidths of resonances in the 1D ^{1}H NMR experiment were determined using the deconvolution routine in TopSpin 3.1. The transverse Paramagnetic Relaxation Enhancement rate (PRE) was defined as a slope of the fitted linear function for the first two points of the titration, for which the attenuation was the largest[41].

Determination of diffusion coefficients Diffusion coefficients were measured by PGSTE NMR with a stimulated spin echo sequence with bipolar gradients, one spoil gradient and a 3-9-19 water suppression scheme[63]. The maximum gradient strength of the probe was 57.7 G/cm. The diffusion delay was set to 200 ms, while the gradient length was 2 ms long and varied in intensity between 2% and 95% of the maximum gradient strength in 64 steps. Spectra were measured with 256 number of scans. 2D DOSY plots were generated using TOPSPIN 3.1. Non-overlapping resonances and showing pure monoexponential decay were used to extract the diffusion coefficient of the associated species by fitting to the appropriate Stejskal-Tanner equation[64] using an in-house fitting procedure implemented in MATLAB.

C-type lectin binding We used plant lectin, Concanavalin A, to assess C type lectin binding capability of the PGN drug delivery complexes. Since calcium ions are required for Concanavalin A binding, samples of the PGN derivatives were prepared with 8 mM glycopeptide, 100 mM DMPC and 200 mM DHPC concentrations in 100 mM NH_4OAc buffer and 2 mM $CaCl_2$ as a reference without and with the addition of Concanavalin A (1 mM).

Results and Discussion

To gain insight into the interactions between the PGN derivatives with the lipid bilayer, we investigated their DMPC-DHPC bicelle model formulations. In order to focus on the interactions

between the glycopeptide and the lipid molecules, the concentrations of the long chain lipid DMPC (100 mM) were applied in a ca. tenfold excess compared to the derivatives (ca. 8 mM). The ^{1}H NMR spectra of the formulations are dominated by the lipid signals in the aliphatic region, only the amide groups signals of the PGN derivatives are present while in the low field ^{1}H NMR region. The signals of the fatty acid chains of DMPC and DHPC are somewhat separated with the terminal methyl group fully resolved, but the resonances of the polar head groups are in complete overlap. Despite using non-deuterated lipids, a number of peptide resonances were completely free from overlap with the larger lipid signals in the aliphatic region as illustrated in the ^{1}H NMR spectrum of D-Ad$_1$Tp in supplementary Figure 1. These non-overlapping resonances in the aliphatic region and the amide signals were assigned and their T_1 or T_2 relaxation times needed for the evaluation of STD and PRE data were determined. It was, however, not possible to detect STD effects for these reporter resonances in the aliphatic region, because STDs have only a fraction of the original signal intensity and drown in the presence of the larger lipid signals. Also, at high paramagnetic ion concentrations, T_2 relaxation times could only be estimated from linewidths in the aliphatic region.

Detection of the interaction by monitoring the sign of the transient NOE. Since the ^{1}H NMR spectrum did not reveal significant line broadening of the peptide signals, we recorded 2D NOESY spectra to determine the sign of the NOEs, which is dependent on the global motional characteristics of the assembly and thus the size of the molecular species. Positive NOEs were detected in aqueous solutions and large, negative NOEs were observed in the presence of the bicelles as depicted in supplementary Figure 2. Observation of the NOE sign change from positive to negative indicated interaction of the PGN derivatives with the lipid bilayer. As a control, we used *N*-acetyl-D-glucosamine (NAG), which is an uncharged polar molecule and therefore expected to have little or no interaction with the fatty acid sidechains of the lipid molecules. For NAG, weak positive NOEs were observed both in aqueous solution in the presence of bicelles as shown in supplementary Figure 2e.

Only a single set of resonances were observed for the PGN derivatives in the presence of bicelles, which indicates that the molecules are in fast exchange between the lipid bilayer and the aqueous solution on the chemical shift time scale. The detected NOEs under fast exchange condition are

transferred NOEs[36] carrying information on the bound conformation. No intermolecular NOE contacts between the PGN derivatives and the bilayer were detected in the NOESY or the ROESY experiment. This is, however, not unusual for molecules with weak to intermediate affinity to membranes[30].

Thus, the PGN derivatives are partially bound to the bilayer and partially solvated in the aqueous phase in a dynamic equilibrium. In a liposome based delivery system to be used in a vaccination context, the PGN derivatives would be likely in part intercalated into the lipid bilayer and in part entrapped in the inner aqueous compartment.

Characterization of the membrane associated conformation with transferred NOEs. In order to get an insight into the range of conformations available for the PGN derivatives in the lipid bilayer bound state, we used transferred NOEs detected (Supplementary Table 1) in the presence of bicelles at room temperature to calculate the structures associated with the membrane. For D-Ad_1Tp and L-Ad_1Tp, 25 and 14 ^{1}H-^{1}H distances were extracted, respectively, while for Man-D-Ad_1Tp and for Man-L-Ad_1Tp the number of distances was 26 in both cases. The calculated ensembles are shown in Figure 1.

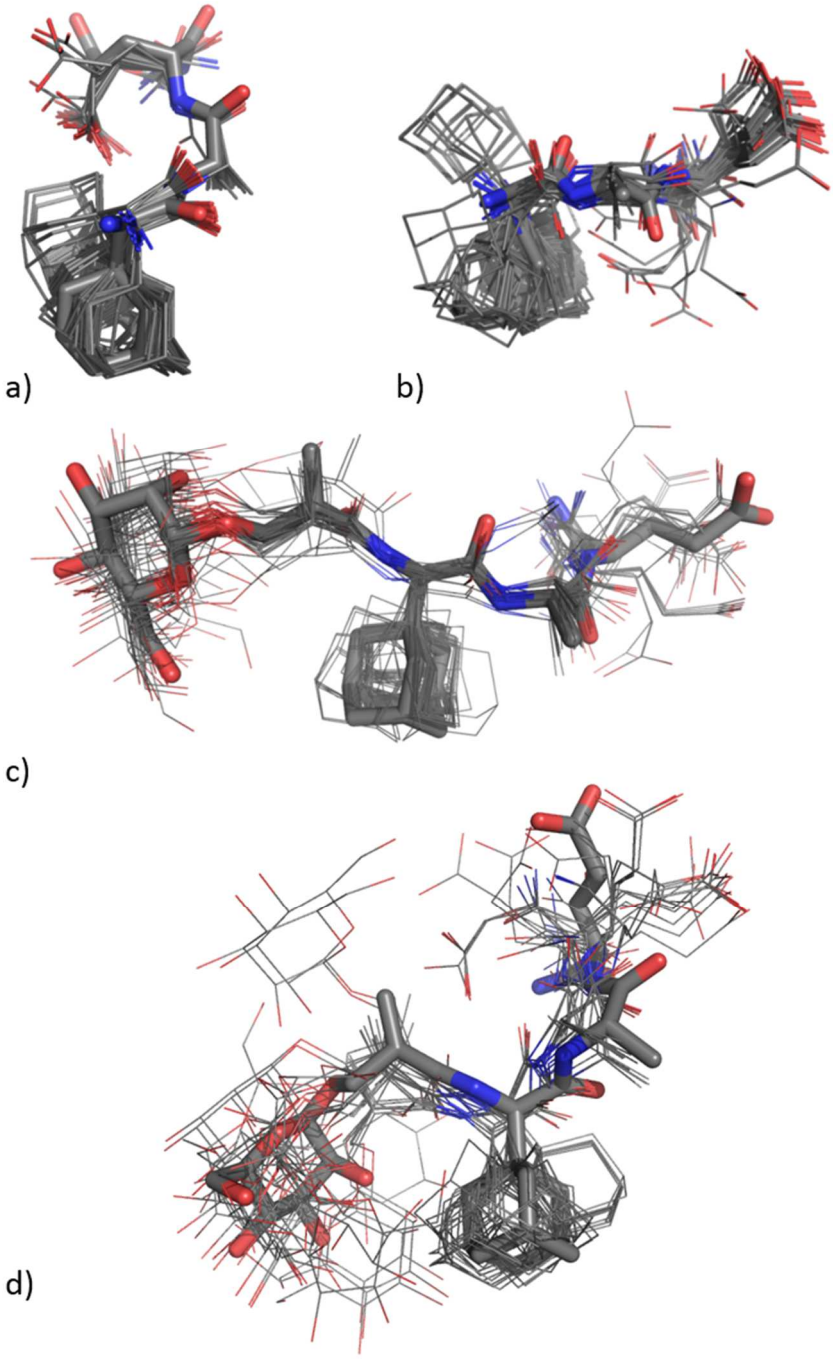

Figure 1. The ensemble of conformations calculated using transferred NOEs for a) D-Ad_1Tp, b) L-Ad_1Tp, c) Man-D-Ad_1Tp and d) Man-L-Ad_1Tp. The average structure is shown in sticks.

The distance restraints derived from transfer NOEs do not determine a single conformation, but rather a range of structures. However, certain trends can be observed. For the non-mannosylated derivatives, the backbone was more or less extended for the majority of L-Ad_1Tp structures (Figure 1a), while for D-Ad_1Tp the C-terminus tends to bend back to the N-terminus (Figure 1b). This bent conformation in

D-Ad_1Tp is enforced by a series of unique restraints from the Ala-NH to the Ada side-chain (denoted in bold in Supplementary Table 1). While the structures of the non-mannosylated derivatives depicted in Scheme 1 show neutral forms, in aqueous solution the peptide termini are likely zwitterionic, thus this bent conformation is likely driven by an intramolecular electrostatic contact between the N terminal amine group and C termini carboxyl group of the derivative.

In the case of the mannosylated derivatives, the transfer NOEs define extended conformations for Man-D-Ad_1Tp, while Man-L-Ad_1Tp displayed structures with a somewhat bent backbone with two of the conformations displaying a close contact between their termini as shown in Figure 1c and d. We note that the structures of the mannosylated derivatives in Scheme 1 are depicted in neutral forms, while in aqueous solution ionized states are likely present with negative charge in the carboxyl group at the C terminal while the N termini of the parent compounds are capped with a neutral, albeit polar mannose group. In the strongly bent subpopulation of Man-L-Ad_1Tp, the hydroxyl groups of the mannose and the D-iGln carboxyl group are close enough for a hydrogen bonding interaction, which is absent for Man-D-Ad_1Tp. For Man-L-Ad_1Tp, the restraints that are responsible for the bent conformations primarily involve NOEs from the Ala-NH group and the D-iGln side-chain to the methyl group of the Lnk residue (denoted in bold in Supplementary Table 1).

Localization and mapping of the orientation within the bilayer via STD and PREs. While both STDs and PREs can be analyzed to yield quantitative structural[38], thermodynamic[65] or kinetic[66] properties, we performed a simpler qualitative evaluation aiming at a complementary epitope mapping of the lipid associated and the solvent accessible parts of the investigated molecules.

STD spectroscopy We performed STD experiments to characterize the orientation of the derivatives in the bilayer. We observed that irradiation at the lipid tail (terminal methyl group) and close to the lipid head (glycerol CH) groups resulted in different STD amplification patterns. Similar effects have been reported for amantadine in isotropic bicelles[30], whereby different STD amplification factors were observed depending on the lipid groups chosen to be saturated. This effect is likely due to the fact that the spread of saturation is not isotropic throughout the bicelle as a result of inefficient spin diffusion. This phenomenon allowed determination of not only the interacting surface of the derivative, but also

the part of the lipid where the saturation is transferred from. Hence, the STD experiment in effect were used to mapping the position of the molecules within the lipid bilayer similarly to the case of amantadine[30].

We performed two types of STD experiments for each derivative as shown in Figure 2: in one experiment the terminal DMPC methyl signal was saturated and in a second experiment the resonance of the 2'CH group of the glycerol backbone representing the overlapping signals of DMPC and DHPC molecules close to the lipid head was irradiated. Identical reference experiments were performed using the aqueous samples of the PGN derivatives, which produced no signal (data not shown). Other lipid resonances were in overlap with the peptide signals that was too strong to allow selective saturation. Only the amide group STDs of the peptides were evaluated as the weak STD signals in the aliphatic region was drowned out by the intense signals from the lipid molecules preventing their detection. The T_1 relaxation times for the corresponding amide resonances were suggested as a correction factor for the final STD amplification factors[60]. However, as the T_1 relaxation times (supplementary Table 2) were very similar to each other for a given derivative, thus they did not affect significantly the STD amplification factors (supplementary Table 3).

Looking at the STD spectra one important qualitative observation can be made at this stage. For the non-mannosylated tripeptides no or very little STD signal was obtained when the lipid tail was irradiated as compared to experiments with irradiation close to the lipid head groups (except for a small signal at D-iGln-NH in D-Ad$_1$Tp). This indicates that the non-mannosylated compounds are not in contact with the inner parts of the bilayer. For the mannosylated compounds, STD signals were detected in both experiments, which appear to imply that the mannosylated derivatives are more immersed into the bilayer than their parent compounds.

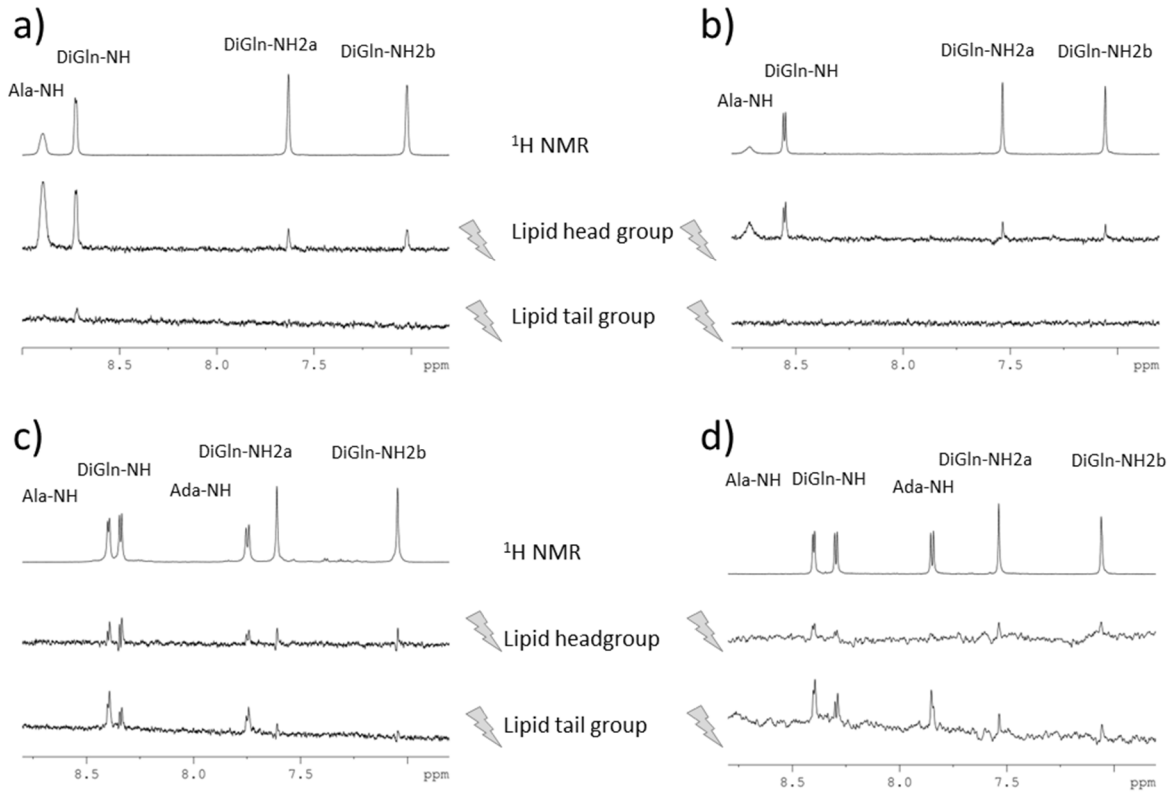

Figure 2. STD with selective irradiation of the resonances of the lipid molecules for compounds a) D-Ad_1Tp, b) L-Ad_1Tp, c) Man-D-Ad_1Tp and d) Man-L-Ad_1Tp: the upper trace shows the reference ^{1}H NMR spectrum of the amide signals, middle trace shows selective irradiation close to the lipid head group (DMPC/DHPC glycerol 2'-CH), lower trace shows selective irradiation of the lipid tail (DMPC 14-Me).

Mapping of the STD amplification factors on the structures as shown in Figure 3 allows qualitative characterization of the location and orientation of the derivatives within the lipid bilayer. Two major conclusions can be drawn. First, the STD signal intensity observed for the sidechain D-iGln-NH_2 groups is less intense than the STD for the other groups. Also, it is less intense with lipid tail irradiation than with saturation close to the lipid head group. This indicates the D-iGln residue does not seem to be in close contact with the bilayer. Second, when resonances close to the lipid head groups were saturated, the most intense STD signal is detected at Ala-NH group for the non-mannosylated compounds, while the Ada-NH moiety received most saturation for the derivatives with mannose groups. Since the lipid resonances dominate the aliphatic region, the mannose and adamantyl groups

are in effect invisible with STD mapping. The Ala-NH and Ada-NH groups are the closest to the adamantyl moiety with observable STDs to serve as reporter groups. These groups displaying strongest STDs thus indicate that the adamantyl group is inserted into the bilayer deepest, at least at the level of the glycerol moiety.

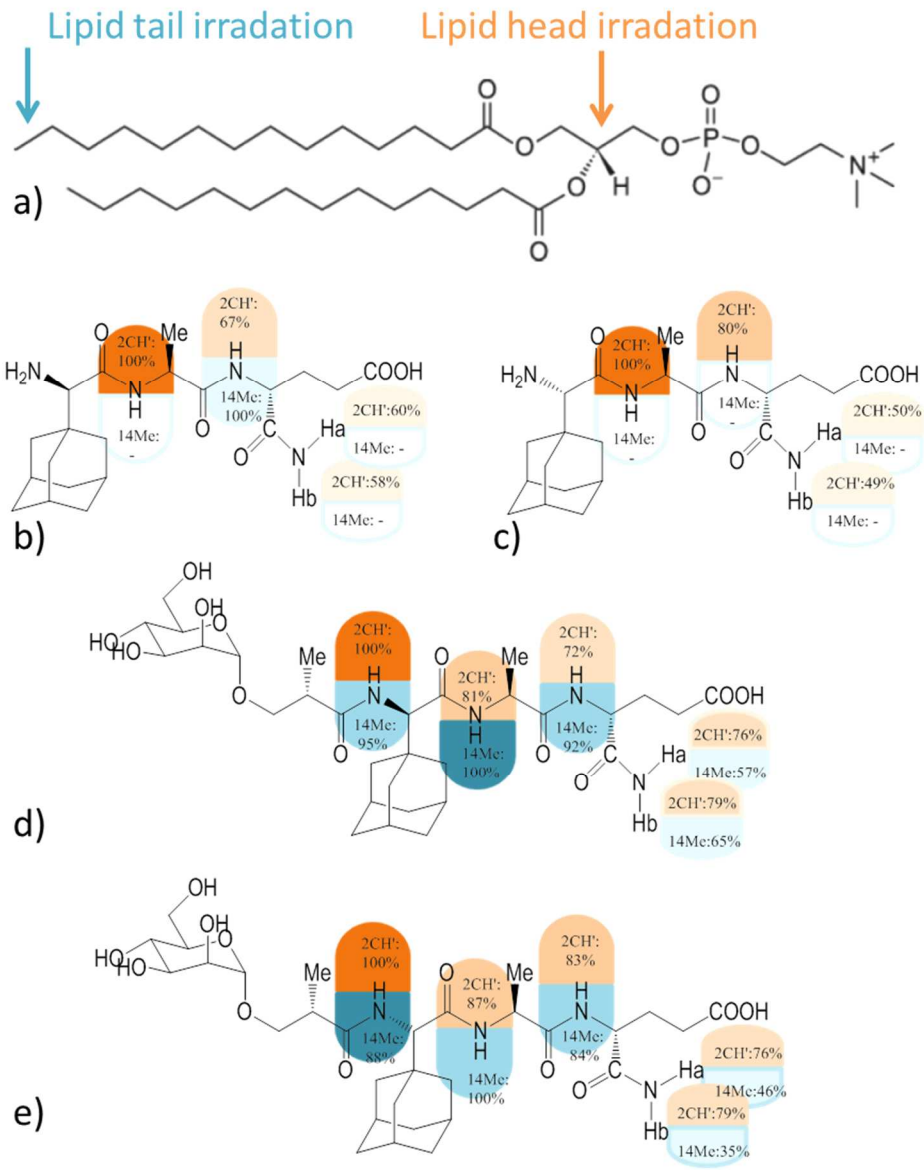

Figure 3. STD signal intensities mapped down onto the structure for compounds a) D-Ad$_1$Tp, b) L-Ad$_1$Tp, c) Man-D-Ad$_1$Tp and d) Man-L-Ad$_1$Tp. The upper value indicates the STD intensity with irradiation close to the lipid head group, while the lower value shows the STD signal with lipid tail saturation.

To conclude the findings of the STD studies, the non-mannosylated parent compounds interact only with the upper layer of the lipid bilayer, while the derivatives with mannose groups appear to be more immersed into the membrane. In all cases the PGN fragment cargo is closest to the surface according to low STDs on D-iGln-NH_2 groups.

Water soluble paramagnetic probes. In order to investigate the parts of the PGN derivatives that are not visible using STD due to dominance of strong lipid resonances in the aliphatic region, that is, the adamantyl group and the mannosyl group, we used PRE induced by water soluble paramagnetic probes, specifically by manganese(II) ions. We monitored PRE-induced bleaching effects during a titration with paramagnetic ions for various reporter groups in the derivatives as shown in Figure 4.

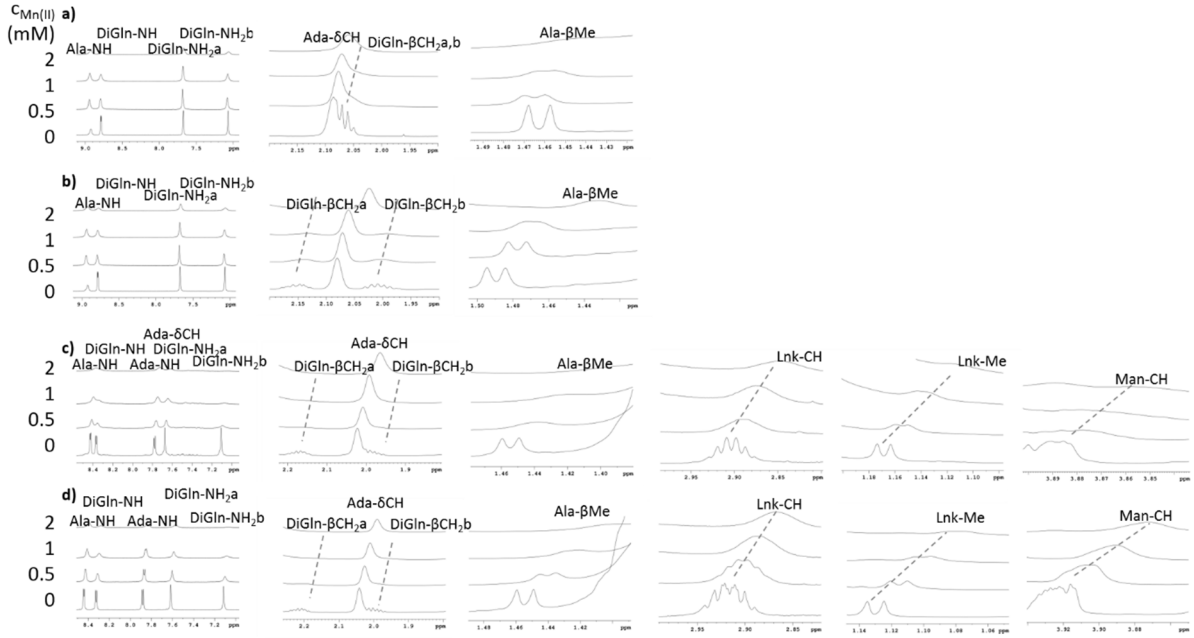

Figure 4. Broadening of ^{1}H NMR resonances during the titration with paramagnetic manganese(II) ions for a) D-Ad_1Tp, b) L-Ad_1Tp, c) Man-D-Ad_1Tp and d) Man-L-Ad_1Tp.

We also quantified the bleaching effect defined as the attenuation of T_2 relaxation times (Figure 5), which were either as measured in CPMG experiments or estimated from linewidth during the titration (Supplementary Table 4). In the case of many resonances, the T_2 relaxation times did not decrease linearly with increasing paramagnetic ion concentrations, the change between the first two points of titration (for which no paramagnetic ion was present followed by addition of 0.5 mM manganese(II) ions) was the largest, while for the remaining titration points diminishing reduction of T_2 relaxation

times was observed. For this reason, the slope of the linear function fitted for the first two points was used to define the attenuation of the T_2 relaxation times.

We found that the resonances of D-iGln-βCH_2 and that of the mannose group (Figure 4, columns 2 and 6) quickly decline (large T_2 attenuation, Figure 5), which indicate that these terminal groups are solvent exposed. Such localization of D-iGln on the surface also is in agreement with result of the STD epitope mapping. In contrast, the signals of the adamantyl moiety, Ada-δCH, are hardly affected by addition of the paramagnetic ions and display similar linewidth and intensity at high or low paramagnetic ion concentrations (Figure 4, column 2). This indicates that the adamantyl group is immersed in the lipid bilayer, which protects it from relaxation effects of the water solvated paramagnetic ions (low T_2 attenuation, Figure 5). Between the two extremes, the attenuation is gradually changing: the resonances of Ala-βMe group (Figure 4, column 3) and that of the linker residue (Lnk) (Figure 4, column 4) show intermediate bleaching effects (Figure 5). Comparison of the bleaching effects of the amide resonances in Figure 5 show that for all derivatives the D-iGln-NH shows the fastest initial decrease in T_2 relaxation times (large T_2 attenuation) resulting in broadening of linewidth and loss of intensity upon increasing paramagnetic ion concentration (Figure 4, column 1). This further confirms the solvent exposure of the PGN fragment cargo.

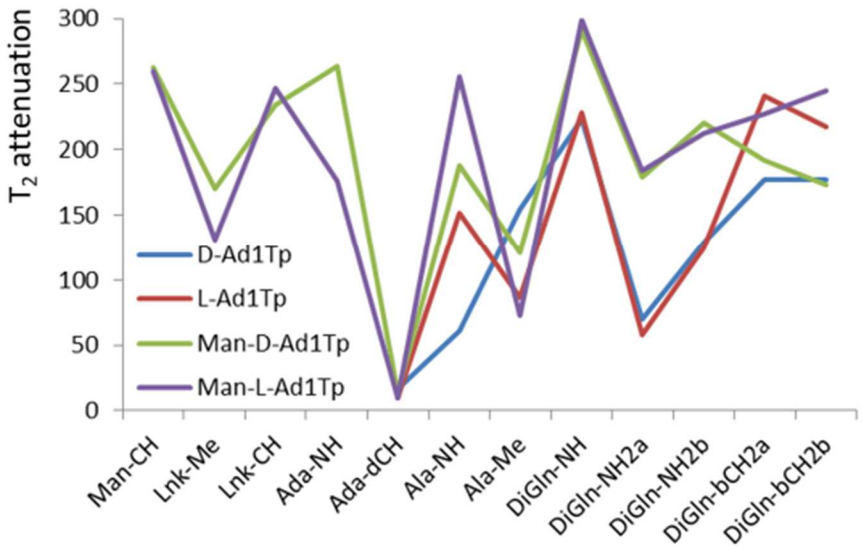

Figure 5. Attenuation of the relaxation times upon addition of paramagnetic ions as measured by the slope of the linear function fitted for T_2 relaxation times at the first two points of the titration, that is, at zero and 0.5 mM of paramagnetic ion concentrations.

The PRE data indicates that the targeting mannosyl group and the PGN fragment cargo of the derivatives are available for interaction with receptors, while the adamantyl group is intercalated into the lipid bilayer and serves as an anchor to the membrane. These findings are in line with previous observations for related PGN-based adjuvants with adamantyl-2-yl attachment[67], whereby the mannose group was found on the surface of liposomes by Dynamic Light Scattering and Atomic Force Microscopy. By comparison, amantadine was located in the head group region of phosphocholine membranes at the surface of the lipid bilayer by neutron and X-ray diffraction[28], however, occasionally it was also shown to penetrate the deeper regions of the bilayer, which was also confirmed by EPR[29]. In a liquid state NMR study[30], it was possible to perform irradiation of a number of lipid resonances enabling more precise mapping of amantadine by STD. This showed that the drug is distributed in a wide region starting from in the glycerol CH_2 group near the negatively charged phosphate group and the entire hydrocarbon region. Thus, it appears that the adamantane group can position itself in various regions of the membrane. Surface location of amantadine is probably driven by electrostatic attraction between negatively charged phosphate head groups of the lipids and the positive charge at the amine group on amantadine similarly to the case of the non-mannosylated PGN derivatives, which also have a positively charged terminal amine group. Deeper penetration of amantadine into the aliphatic lipid chain region is likely driven by the strongly hydrophobicity of the adamantane group. This interaction might also become more dominant for the mannosylated derivatives, in which the charged amine groups at the N termini are capped by neutral mannose groups.

Determination of the in-situ encapsulation efficiency by measurement of translational diffusion. Changes in translational diffusion coefficients in the presence of bicelles compared to the aqueous solution provided another piece of evidence of the interaction. DOSY plots are depicted in the PGN derivatives in bicelles in Figure 6, which show a significant drop in the translational diffusion coefficient compared to the aqueous solution. The diffusion coefficient of NAG in aqueous buffer

solution is very similar to its value in the presence of bicelles (Figure 6e) except for a small difference probably due to different sample viscosity.

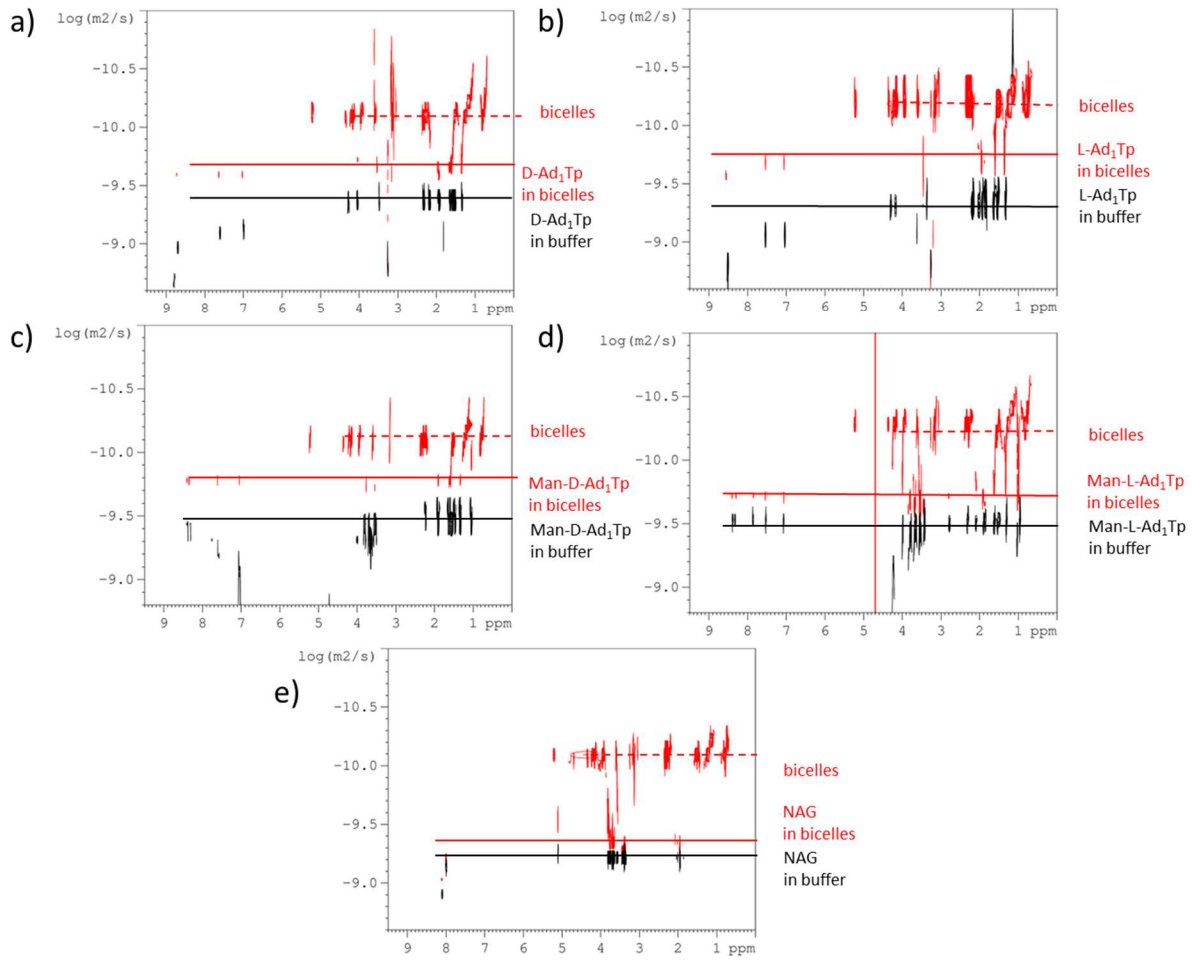

Figure 6. DOSY plot of compounds at 25ºC a) D-Ad$_1$Tp, b) L-Ad$_1$Tp, c) Man-D-Ad$_1$Tp d) Man-L-Ad$_1$Tp and e) for NAG in the presence (red) and absence (black) of bicelles.

A single set of signals was observed in the diffusion dimension for each species; thus, the derivatives are in fast exchange not only on the chemical shift scale, but also on the diffusion time scale. This provided the opportunity to use the diffusion coefficients to quantify the lipid encapsulation efficiency.

The decays of the peptide signals generated in the diffusion experiment and used in a numerical fitting are mono-exponential when plotted against the square of the gradient strength (supplementary Figure 3), which indicates that the exchange regime on the diffusion time scale is fast compared to the inverse of the diffusion delay (200 ms). Assuming a two-site exchange of the derivatives between the bicelle-

bound and free solvated forms, we can use the diffusion constants of the different molecular species to estimate the fraction of peptides bound to the lipid bilayer and calculate the encapsulation efficiency[30, 68-69]. Under fast exchange conditions the observed diffusion coefficient is a population average of the diffusion coefficients of the molecules freely diffusing in the aqueous solution and that of the molecules bound to the bicelle:

$$D_{obs} = p_{lipid} D_{bicelle} + (1 - p_{lipid})D_{free}$$

where

D_{obs}: observed diffusion coefficient of the compound in the presence of bicelles

$D_{bicelle}$: diffusion coefficient of the bicelle as measured on the DMPC terminal methyl signal

D_{free}: diffusion coefficient of the compound in the aqueous phase

p_{lipid}: fraction of compounds encapsulated in lipid bicelles

Furthermore, the measured diffusion coefficients of the PGN derivatives is corrected for the obstruction effect arising from the reduced volume available for the assemblies to diffuse, thus obtaining the diffusion coefficient at infinite dilution:

$$D_{obs} = D_{measured} (1 - 2k\Phi)$$

where D_{obs} is the diffusion coefficient at infinite dilution

$D_{measured}$ is the measured diffusion coefficient

k is a shape dependent factor assuming near spherical shape of the bicelles[70]

Φ is the volume fraction, which was approximated by the weight fraction of phospholipids excluding monomer DHPC[30, 48].

Finally, in order to account for different viscosities in the aqueous and the bicelle solutions, a correction factor was used based on the ratio of the diffusion coefficients of water in the two solutions (234 $\mu m^2/s$ in water and 253 $\mu m^2/s$ in bicelles with q=0.5[68]).

Thus, the fraction of the compounds incorporated in the lipid bicelles (p_{lipid}) and their partition coefficient (K_p) can be determined as follows:

$$p_{lipid} = (D_{free} - D_{obs}) / (D_{free} - D_{lipids})$$

$$K_p = p_{lipid} / (1-p_{lipid})$$

Numerical diffusion constants determined by fitting and encapsulation efficiencies at 25°C and at 37°C are shown in Table 1 and 2. The values are between 19% and 49 % at room temperature and 42% and 56% at 37°C. By comparison, the incorporation efficiency of peptidoglycan monomer[71] fragment isolated from Gram negative bacteria into lipid bilayers is 16 to 23 % using an HPLC based method[72]. Lipid entrapments of 22% and 35% were determined for isomers of the adamantyl compounds with adamantyl-2-yl attachment, for D-Ad_2Tp and L-Ad_2Tp[72], respectively (depending on the method of preparation, 23% and 30% were also measured,). The lipid-to-peptide ratio in these preparations were rather closer to 1:1, than 10:1 as in the NMR investigations, which could explain lower incorporation values. Membrane partitioning (K_p) of spin labelled amantadine was found to be 11.2 at 45°C in DMPC vesicles using EPR[29], 27.6 in DMPC and 37.8 in POPC lipids using NMR[30], much larger than the partition coefficients determined here. Amantadine is, however, much smaller in size than the derivatives studied here and has only a single charged group.

Table 1. Diffusion coefficients determined in the aqueous and the lipid phase and derived lipid bound fraction and partition coefficients at 25°C.

Compounds	**D_{free} (10^{-12}) (m^2/s)**	**D_{obs} (10^{-12}) (m^2/s)**	**p_{lipid}**	**K_p**
D-Ad_1Tp	383 ± 1.7	215 ± 7.1	0.32	0.47
L-Ad_1Tp	376 ± 1.7	162 ± 0.1	0.49	0.96
Man-D-Ad_1Tp	268 ± 4.3	151 ± 4.8	0.19	0.23
Man-L-Ad_1Tp	283 ± 7.7	185 ± 3.5	0.24	0.32
NAG	536 ± 17.3	388 ± 2.3	0.01	0.01

Table 2. Diffusion coefficients determined in the aqueous and the lipid phase and derived lipid bound fraction and partition coefficients at 37°C.

Compounds	D_{free} (10^{-12}) (m^2/s)	D_{obs} (10^{-12}) (m^2/s)	p_{lipid}	K_p
D-Ad_1Tp	622 ± 10.0	304 ± 8.3	0.51	1.05
L-Ad_1Tp	537 ± 15.8	252 ± 11.2	0.56	1.26
Man-D-Ad_1Tp	480 ± 10.6	288 ± 15.2	0.43	0.75
Man-L-Ad_1Tp	495 ± 12.1	262 ± 15.9	0.42	0.72
NAG	549 ± 9.8	469 ± 20.0	0.02	0.02

By comparing the values, two observations may become relevant for the design of these molecules. First, we note that the non-mannosylated compounds are incorporated more efficiently into the bilayer at both temperatures, while attachment of the mannose group reduces the incorporation efficiency. Taking into consideration the results obtained regarding conformation, localization and orientation of the derivatives in the bilayer, we propose the following molecular interpretation for this finding. The non-mannosylated derivatives are in zwitterionic forms containing an ionized N-terminal amine and a C-terminal carboxyl group. The interaction of these compounds could involve electrostatic contacts from their charged termini to the positively charged choline groups and the negatively charged phosphate groups in the lipid molecules. In contrast, the mannosylated derivatives bear only a negatively charged C-terminus as the N-terminus is capped by the neutral, albeit polar mannose moiety making only one ionic interaction possible with the lipids. The presence of two charged groups on the non-mannosylated compounds likely prevents deeper incorporation into the lipid bilayer explaining the observed STD patterns. However, these two electrostatic interactions in the upper layer of the assembly can reasonably be assumed to result in a stronger interaction with the lipid molecules relative to the mannosylated compounds, where only one strong electrostatic interaction present, thus leading to stronger incorporation efficiencies of the non-mannosylated compounds.

We have shown[34], that the glycopeptides's co-stimulation activity to LPS on macrophages was further increased by the incorporation of the compounds into phosphatidylcholine lipid bilayers. Only L-Ad_1Tp and Man-L-Ad_1Tp were investigated in the *in vitro* assay for this effect. Albeit that the adjuvant effect of Man-L-Ad_1Tp both in aqueous solution and in liposomes was better, the *relative* increase of the adjuvant effect upon incorporation of L-Ad_1Tp compared to the aqueous solution was

more significant. Thus, L-Ad_1Tp profited more from the lipid delivery system than Man-L-Ad_1Tp and this may be related to the higher lipid incorporation efficiency of the non-mannosylated compound compared to the derivative with the mannose group.

Secondly, we may observe that the chirality of the adamantyl group influence the incorporation efficiency, which might be correlated with the membrane associated conformation in the following way. D-Ad_1Tp interacts weaker with the lipid bilayer than L-Ad_1Tp with a most pronounced difference at low temperature (32%vs 49%) and a smaller distinction at high temperature (51% vs 56%). At room temperature, D-Ad_1Tp adopts a bent conformation, which may be attributed to an ionic interaction between the charged C and N-terminal groups. Such an intramolecular contact might prevent or at least compete with the charged terminals engaging in intermolecular interactions with the lipid molecules and this could explain the weaker encapsulation into the bilayer. For the mannosylated derivatives, the encapsulation between the diastereoisomers differs less at room temperature (19% vs 24%) and is similar at 37°C (43% vs 42%). A subpopulation Man-L-Ad_1Tp determined at room temperature also displayed a bent backbone enabled by an intramolecular hydrogen bond between the termini. Similar to the reasoning above, these groups may not be fully available for intermolecular interactions with polar lipid groups, which might explain lower encapsulation. This observation and explanation is in agreement with reports showing that lipophilicity of drug molecules has been found to be affected by the formation of intramolecular hydrogen bonds, which shields the hydrogen bond donor and acceptor groups from intermolecular interactions[73].

Binding to CLRs. The adjuvant activity of the adamantylated PGN derivatives likely involves interaction with multiple receptors of the innate immune system, however, these receptors have not yet been unequivocally clarified. Targeting via the mannosyl group requires recognition by cell surface CLRs that facilitate internalization of microbes by binding of terminal mannose groups and could therefore contribute to the increased uptake and to the augmentation of the adjuvant effect. Targeting was evidenced[16] by the more effective adjuvant activity of the derivatives with the mannose targeting group than that of the non-mannosylated parent compounds.

The interaction of CLRs with the mannosyl targeting group can be mimicked by plant lectins such as Concanavalin A (Con A). Specificity of carbohydrate-lectin interactions are often studied using Con A with detection of the changes in hydrodynamic radius by Dynamics Light Scattering[74]. Here we used NMR diffusion experiments to detect changes in translational diffusion upon addition of Con A. In order to see if the mannosyl group is available for binding to endogenous cell surface receptors, we added 1 mM Con A to the bicelle solutions of the PGN derivatives in the presence of calcium ions and monitored the translational diffusion of the peptides. In both cases decrease in the diffusion constants was observed (Figure 7), which was also accompanied by chemical shift changes.

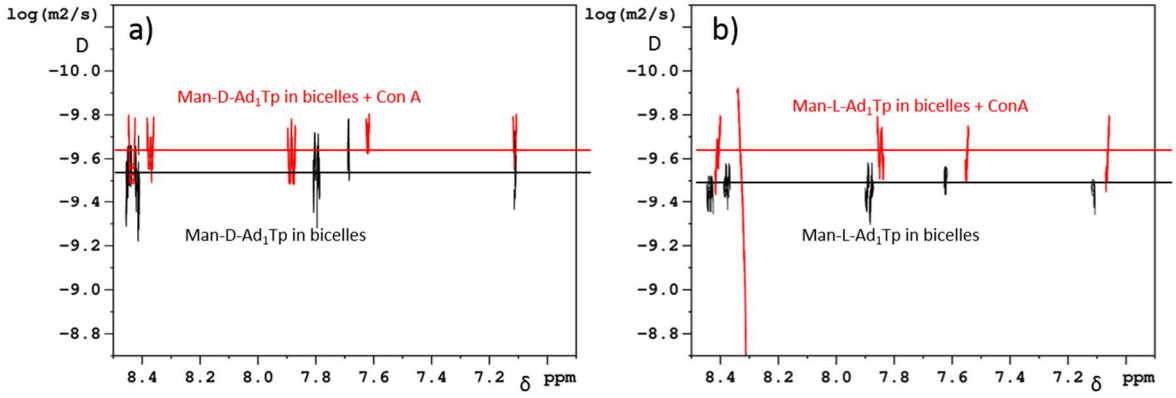

Figure 7. Comparison of DOSY plots for a) Man-D-Ad$_1$Tp and b) Man-L-Ad$_1$Tp in the presence of bicelles (black) and after addition of 1 mM Con A (red).

Due to fast exchange between the various glycopeptide containing species, only a single apparent diffusion coefficient is observable in the DOSY spectrum, which is a population averaged value of the diffusion coefficients of the individual complexes present. The observed decrease in translational diffusion coefficient of the PGN derivatives may be attributed to the glycopeptides crosslinking bicelles around the lectin, which is able to bind up to four mannosyl groups. This might indicate that the mannosyl moiety of both derivatives incorporated into bilayers are available for binding to cell surface CLRs.

Conclusions

Adamantylated PGN derivatives without and with mannose targeting groups were investigated in lipid model membranes using NMR spectroscopy. Lipid incorporation efficiencies between 19-49% and 42-56% were found at room temperature and at 37ºC, respectively. The parent compounds showed higher lipid encapsulation than their mannosylated conjugates. Immune co-stimulation activities of the derivatives *in vitro* were amplified upon incorporation into liposomes and more so for the non-mannosylated derivatives than for the compounds with mannose groups, which may be attributed to differences in lipid incorporation efficiencies.

It was also found that the non-mannosylated compounds are only in contact with the upper parts of the bilayer, while the derivatives with mannose groups penetrate deeper in the bilayer. In all cases the PGN cargo fragments and the mannosyl groups of the glycopeptide derivatives are close to the surface of the bilayer. These observations can be rationalized by considering possible electrostatic interactions between the charged groups of the derivatives and that of the lipid molecules. The membrane interaction was found to be influenced by the chirality of the adamantyl group and appeared to be correlated with the membrane associated conformations. This effect could be related to the availability of the charged or polar groups for intermolecular interactions with the lipid molecules and thereby explain differences in incorporation efficiency.

On the basis of the findings by NMR, we propose that the mannosylated adamantylated PGN derivatives in liposome formulations can intercalate themselves into the lipid bilayer, while also present in the inner aqueous compartment due to their solubility in water. In the bilayer bound arrangement, which is depicted in Scheme 2, the targeting mannosyl group is able to interact with cell–surface CLRs, while the PGN fragment cargo is available for contact with cell surface or, after internalization, cytosolic receptors. Thus, we show that different functional groups of the PGN derivatives designed for liposomal delivery are located on the surface of the lipid assembly in an arrangement that enables interactions with the targeted receptors. The conformations of the molecules solvated in the inner aqueous compartment might different than that of the membrane associated molecules.

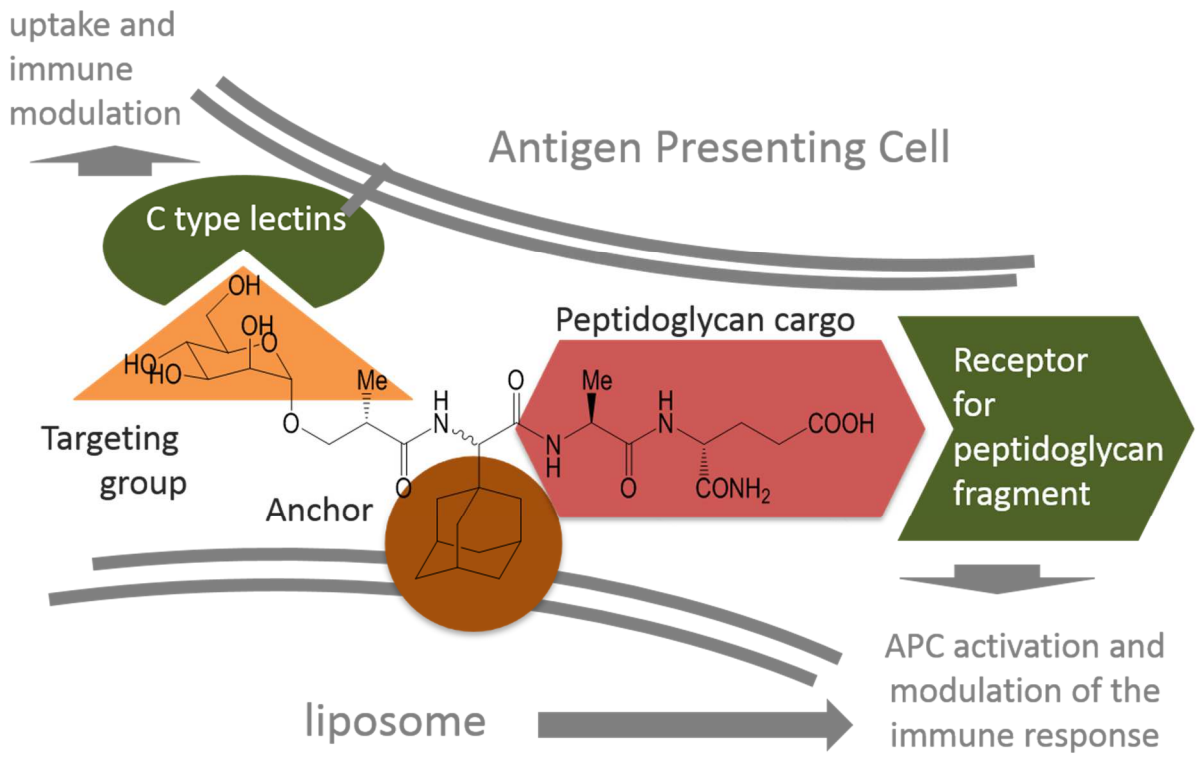

Scheme 2. Proposed interactions of the mannosylated PGN derivatives embedded in liposome with cell surface receptors of Antigen Presenting Cells (APC). Figure is for illustration of the mutual arrangement of the components that are not to scale.

By elucidating the molecular details of membrane interactions of adamantylated PGN derivatives, we have taken the first steps towards the understanding their lipid formulations, which will enable further modifications to improve efficiency of membrane encapsulation and adjuvant activity of this type of molecules.

Author Contributions

The manuscript was written through contributions of all authors. All authors have given approval to the final version of the manuscript.

Acknowledgement

R.R. and S.T. wish to thank the Croatian Science Foundation for support (project IP-2014-09-7899). M.M.K. and R.J. acknowledge the support from Slovenian Research Agency (program no. P4-0176). F.C. thanks the Erasmus Mundus Peace fellowship. D.S. thanks the Research Foundation-Flanders (FWO-Vlaanderen) for a postdoctoral research fellowship and a research grant (1.5.133.13N). K.F. acknowledges the support of the Marie Curie Career Integration Grant (303917 PGN-INNATE) and the Research Grant from the Research Foundation-Flanders (1508414N and 1525517N). János Bolyai Research Scholarship of the Hungarian Academy of Sciences (BO/004333/18/7) and the New National Excellence Program of Debrecen University (ÚNKP-19-4 Bolyai+). This research was supported by the National Research, Development and Innovation Office of Hungary (grant NKFI/OTKA NN 128368). We thank Dr Ruža Frkanec and Prof László Szilágyi for stimulating discussions. The 700 MHz equipment in this work was funded from the FFEU-ZWAP initiative of the Flemish Government.

Conflicts of interest: none

Supporting Information

Supplementary Figure 1. ^{1}H NMR spectra of D-Ad$_1$Tp complete with assignment at 37^{o}C and 700MHz.

Supplementary Figure 2. NOESY spectra of the PGN derivatives in bicelles

Supplementary Table 1. T_1 relaxation times of the amide resonances

Supplementary Table 2. STD amplification factors corrected with T_1 relaxation times

Supplementary Table 3. T_2 relaxation times for the amide resonances during the Mn(II) ion titration

Supplementary Table 4 Summary of the signal intensities of the transfer NOEs for the PGN derivatives.

Supplementary Figure 3. Stejskal-Tanner plots of PGSTE signal decays

References

1. Harandi, A. M.; Medaglini, D.; Shattock, R. J.; Working Grp Convened, E., Vaccine adjuvants: A priority for vaccine research. *Vaccine* **2010,** *28* (12), 2363-2366.

2. Oleszycka, E.; Lavelle, E. C., Immunomodulatory properties of the vaccine adjuvant alum. *Current Opinion in Immunology* **2014,** *28*, 1-5.

3. Coffman, R. L.; Sher, A.; Seder, R. A., Vaccine adjuvants: putting innate immunity to work. *Immunity* **2010,** *33* (4), 492-503.

4. Sorbara, M. T.; Philpott, D. J., Peptidoglycan: a critical activator of the mammalian immune system during infection and homeostasis. *Immunological Reviews* **2011,** *243*, 40-60.

5. Lise, L. D.; Audibert, F., IMMUNOADJUVANTS AND ANALOGS OF IMMUNOMODULATORY BACTERIAL STRUCTURES. *Current Opinion in Immunology* **1989,** *2* (2), 269-274.

6. Myhre, A. E.; Aasen, A. O.; Thiemermann, C.; Wang, J. E., PEPTIDOGLYCAN-AN ENDOTOXIN IN ITS OWN RIGHT? *Shock* **2006,** *25* (3), 227-235.

7. Szilagyi, L.; Pristovsek, P., Structural aspects of peptides with immunomodulating activity. *Mini-Reviews in Medicinal Chemistry* **2007,** *7* (8), 861-870.

8. Ogawa, C.; Liu, Y.-J.; Kobayashi, K., Muramyl Dipeptide and its Derivatives: Peptide Adjuvant in Immunological Disorders and Cancer Therapy. *Current bioactive compounds* **2011,** *7*, 180-197.

9. Girardin, S. E.; Boneca, I. G.; Viala, J.; Chamaillard, M.; Labigne, A.; Thomas, G.; Philpott, D. J.; Sansonetti, P. J., Nod2 Is a General Sensor of Peptidoglycan through Muramyl Dipeptide (MDP) Detection. *Journal of Biological Chemistry* **2003,** *278* (11), 8869-8872.

10. Torchilin, V. P., Recent advances with liposomes as pharmaceutical carriers. *Nature Reviews Drug Discovery* **2005,** *4* (2), 145-160.

11. Sone, S.; Mutsuura, S.; Ogawara, M.; Tsubura, E., POTENTIATING EFFECT OF MURAMYL DIPEPTIDE AND ITS LIPOPHILIC ANALOG ENCAPSULATED IN LIPOSOMES ON TUMOR-CELL KILLING BY HUMAN-MONOCYTES. *Journal of Immunology* **1984,** *132* (4), 2105-2110.

12. Effenberg, R.; Turánek Knötigová, P.; Zyka, D.; Čelechovská, H.; Mašek, J.; Bartheldyová, E.; Hubatka, F.; Koudelka, Š.; Lukáč, R.; Kovalová, A.; Šaman, D.; Křupka, M.; Barkocziova, L.; Kosztyu, P.; Šebela, M.; Drož, L.; Hučko, M.; Kanásová, M.; Miller, A. D.; Raška, M.; Ledvina, M.; Turánek, J., Nonpyrogenic Molecular Adjuvants Based on norAbu-Muramyldipeptide and norAbu-Glucosaminyl Muramyldipeptide: Synthesis, Molecular Mechanisms of Action, and Biological Activities in Vitro and in Vivo. *Journal of Medicinal Chemistry* **2017,** *60* (18), 7745-7763.

13. Jakopin, Ž., Murabutide Revisited: A Review of its Pleiotropic Biological Effects. *Current medicinal chemistry* **2013,** *20*.

14. Ribic, R.; Habjanec, L.; Vranesic, B.; Frkanec, R.; Tomic, S., Synthesis and Biological Evaluation of New Mannose Derived Immunomodulating Adamantyltripeptides. *Croatica Chemica Acta* **2011,** *84* (2), 233-244.

15. Ribic, R.; Habjanec, L.; Vranesic, B.; Frkanec, R.; Tomic, S., Synthesis and Immunostimulating Properties of Novel Adamant-1-yl Tripeptides. *Chemistry & Biodiversity* **2012,** *9* (4), 777-788.

16. Ribic, R.; Habjanec, L.; Frkanec, R.; Vranesic, B.; Tomic, S., Influence of Mannosylation on Immunostimulating Activity of Adamant-1-yl Tripeptide. *Chemistry & Biodiversity* **2012,** *9* (7), 1373-1381.

17. Davies, W. L.; Grunert, R. R.; Haff, R. F.; McGahen, J. W.; Neumayer, E. M.; Paulshock, M.; Watts, J. C.; Wood, T. R.; Hermann, E. C.; Hoffmann, C. E., ANTIVIRAL ACTIVITY OF 1-ADAMANTANAMINE (AMANTADINE). *Science (New York, N.Y.)* **1964,** *144* (3620), 862-3.

18. Oxford, J. S.; Galbraith, A., Antiviral activity of amantadine: a review of laboratory and clinical data. *Pharmacology & Therapeutics* **1980,** *11* (1), 181-262.

19. Danielczyk, W., Twenty-five years of amantadine therapy in Parkinson's disease. *Journal of neural transmission. Supplementum* **1995,** *46*, 399-405.

20. Blanchet, P. J.; Metman, L. V.; Chase, T. N., Renaissance of amantadine in the treatment of Parkinson's disease. *Advances in neurology* **2003,** *91*, 251-7.

21. Kilpatrick, G. J.; Tilbrook, G. S., Memantine. Merz. *Current opinion in investigational drugs (London, England : 2000)* **2002,** *3* (5), 798-806.

22. Francis, P. T., Glutamatergic Approaches to the Treatment of Cognitive and Behavioural Symptoms of Alzheimer's Disease. *Neurodegenerative Diseases* **2008,** *5* (3-4), 241-243.

23. Pinto, L. H.; Holsinger, L. J.; Lamb, R. A., Influenza virus M2 protein has ion channel activity. *Cell* **1992,** *69* (3), 517-28.

24. Griffin, S. D.; Beales, L. P.; Clarke, D. S.; Worsfold, O.; Evans, S. D.; Jaeger, J.; Harris, M. P.; Rowlands, D. J., The p7 protein of hepatitis C virus forms an ion channel that is blocked by the antiviral drug, Amantadine. *FEBS letters* **2003,** *535* (1-3), 34-8.

25. Lipton, S. A., Paradigm shift in neuroprotection by NMDA receptor blockade: memantine and beyond. *Nature reviews. Drug discovery* **2006,** *5* (2), 160-70.

26. Jain, M. K.; Yen-Min Wu, N.; Morgan, T. K.; Briggs, M. S.; Murray, R. K., Phase transition in a lipid bilayer. II. Influence of adamantane derivatives. *Chemistry and Physics of Lipids* **1976,** *17* (1), 71-78.

27. Phonphok, Y.; Rosenthal, K. S., Stabilization of clathrin coated vesicles by amantadine, tromantadine and other hydrophobic amines. *FEBS letters* **1991,** *281* (1), 188-190.

28. Duff, K. C.; Cudmore, A. J.; Bradshaw, J. P., The location of amantadine hydrochloride and free base within phospholipid multilayers: a neutron and X-ray diffraction study. *Biochimica et Biophysica Acta (BBA) - Biomembranes* **1993,** *1145* (1), 149-156.

29. Subczynski, W. K.; Wojas, J.; Pezeshk, V.; Pezeshk, A., Partitioning and Localization of Spin-Labeled Amantadine in Lipid Bilayers: An Epr Study. *Journal of Pharmaceutical Sciences* **1998,** *87* (10), 1249-1254.

30. Wang, J. F.; Schnell, J. R.; Chou, J. J., Amantadine partition and localization in phospholipid membrane: a solution NMR study. *Biochemical and Biophysical Research Communications* **2004,** *324* (1), 212-217.

31. White, K. L.; Rades, T.; Furneaux, R. H.; Tyler, P. C.; Hook, S., Mannosylated liposomes as antigen delivery vehicles for targeting to dendritic cells. *Journal of Pharmacy and Pharmacology* **2006,** *58* (6), 729-737.

32. Kerrigan, A. M.; Brown, G. D., C-type lectins and phagocytosis. *Immunobiology* **2009,** *214* (7), 562-75.

33. Geijtenbeek, T. B. H.; Gringhuis, S. I., Signalling through C-type lectin receptors: shaping immune responses. *Nature Reviews Immunology* **2009,** *9* (7), 465-479.

34. Ribić, R.; Manček-Keber, M.; Chain, F.; Sinnaeve, D.; Martins, J. C.; Jerala, R.; Tomić, S.; Fehér, K., Adamantane containing peptidoglycan fragments enhance the lipopolysaccharide-induced immune response

35. Neuhaus, D.; Williamson, M. P., *The nuclear Overhauser effect in structural and conformational analysis*. Wiley-VCH: 2000.

36. Ni, F., Recent developments in transferred NOE methods. *Progress in Nuclear Magnetic Resonance Spectroscopy* **1994,** *26*, 517-606.

37. Mayer, M.; Meyer, B., Characterization of ligand binding by saturation transfer difference NMR spectroscopy. *Angewandte Chemie-International Edition* **1999,** *38* (12), 1784-1788.

38. Mayer, M.; Meyer, B., Group epitope mapping by saturation transfer difference NMR to identify segments of a ligand in direct contact with a protein receptor. *Journal of the American Chemical Society* **2001,** *123* (25), 6108-6117.

39. Angulo, J.; Nieto, P. M., STD-NMR: application to transient interactions between biomolecules—a quantitative approach. *European Biophysics Journal* **2011,** *40* (12), 1357-1369.

40. Yan, J. L.; Kline, A. D.; Mo, H. P.; Shapiro, M. J.; Zartler, E. R., The effect of relaxation on the epitope mapping by saturation transfer difference NMR. *Journal of Magnetic Resonance* **2003,** *163* (2), 270-276.

41. Al-Abdul-Wahid, M. S.; Neale, C.; Pomes, R.; Prosser, R. S., A Solution NMR Approach to the Measurement of Amphiphile Immersion Depth and Orientation in Membrane Model Systems. *Journal of the American Chemical Society* **2009,** *131* (18), 6452-6459.

42. Solomon, I., Relaxation Processes in a System of Two Spins. *Physical Review* **1955,** *99* (2), 559-565.

43. Clore, G. M.; Iwahara, J., Theory, Practice, and Applications of Paramagnetic Relaxation Enhancement for the Characterization of Transient Low-Population States of Biological Macromolecules and Their Complexes. *Chemical Reviews* **2009,** *109* (9), 4108-4139.

44. Morris, K. F.; Johnson, C. S., DIFFUSION-ORDERED 2-DIMENSIONAL NUCLEAR-MAGNETIC-RESONANCE SPECTROSCOPY. *Journal of the American Chemical Society* **1992,** *114* (8), 3139-3141.

45. Hinton, D. P.; Johnson, C. S., Simultaneous measurement of vesicle diffusion coefficients and trapping efficiencies by means of diffusion ordered 2D NMR spectroscopy. *Chemistry and Physics of Lipids* **1994,** *69* (2), 175-178.

46. Durr, U. H. N.; Soong, R.; Ramamoorthy, A., When detergent meets bilayer: Birth and coming of age of lipid bicelles. *Progress in Nuclear Magnetic Resonance Spectroscopy* **2013,** *69*, 1-22.

47. Mäler, L.; Gräslund, A., Artificial Membrane Models for the Study of Macromolecular Delivery. In *Macromolecular Drug Delivery*, Belting, B., Ed. Humana Press: 2009; Vol. 480, pp 129-139.

48. Andersson, A.; Maler, L., Size and shape of fast-tumbling bicelles as determined by translational diffusion. *Langmuir* **2006,** *22* (6), 2447-2449.

49. Ye, W.; Lind, J.; Eriksson, J.; Mäler, L., Characterization of the Morphology of Fast-Tumbling Bicelles with Varying Composition. *Langmuir* **2014,** *30* (19), 5488-5496.

50. Beaugrand, M.; Arnold, A. A.; Hénin, J.; Warschawski, D. E.; Williamson, P. T. F.; Marcotte, I., Lipid Concentration and Molar Ratio Boundaries for the Use of Isotropic Bicelles. *Langmuir* **2014,** *30* (21), 6162-6170.

51. Glover, K. J.; Whiles, J. A.; Wu, G. H.; Yu, N. J.; Deems, R.; Struppe, J. O.; Stark, R. E.; Komives, E. A.; Vold, R. R., Structural evaluation of phospholipid bicelles for solution-state studies of membrane-associated biomolecules. *Biophysical Journal* **2001,** *81* (4), 2163-2171.

52. Matsumori, N.; Murata, M., 3D structures of membrane-associated small molecules as determined in isotropic bicelles. *Natural Product Reports* **2010,** *27* (10), 1480-1492.

53. Katsaras, J.; Harroun, T. A.; Pencer, J.; Nieh, M. P., "Bicellar" lipid mixtures as used in biochemical and biophysical studies. *Naturwissenschaften* **2005,** *92* (8), 355-366.

54. Björnerås, J.; Nilsson, M.; Mäler, L., Analysing DHPC/DMPC bicelles by diffusion NMR and multivariate decomposition. *Biochimica et Biophysica Acta (BBA) - Biomembranes* **2015,** *1848* (11, Part A), 2910-2917.

55. Vranken, W. F.; Boucher, W.; Stevens, T. J.; Fogh, R. H.; Pajon, A.; Llinas, P.; Ulrich, E. L.; Markley, J. L.; Ionides, J.; Laue, E. D., The CCPN data model for NMR spectroscopy: Development of a software pipeline. *Proteins-Structure Function and Bioinformatics* **2005,** *59* (4), 687-696.

56. Brunger, A. T.; Adams, P. D.; Clore, G. M.; DeLano, W. L.; Gros, P.; Grosse-Kunstleve, R. W.; Jiang, J. S.; Kuszewski, J.; Nilges, M.; Pannu, N. S.; Read, R. J.; Rice, L. M.; Simonson, T.; Warren, G. L., Crystallography & NMR system: A new software suite for macromolecular structure determination. *Acta Crystallographica Section D-Biological Crystallography* **1998,** *54*, 905-921.

57. Linge, J. P.; Williams, M. A.; Spronk, C.; Bonvin, A.; Nilges, M., Refinement of protein structures in explicit solvent. *Proteins-Structure Function and Bioinformatics* **2003,** *50* (3), 496-506.

58. *Discovery Studio Visualiser*, 3.5; Accelrys: 2012.

59. *The PyMOL Molecular Graphics System, Version 1.2*, Schrödinger, LLC.

60. Kemper, S.; Patel, M. K.; Errey, J. C.; Davis, B. G.; Jones, J. A.; Claridge, T. D. W., Group epitope mapping considering relaxation of the ligand (GEM-CRL): Including longitudinal relaxation rates in the analysis of saturation transfer difference (STD) experiments. *Journal of Magnetic Resonance* **2010,** *203* (1), 1-10.

61. Stott, K.; Stonehouse, J.; Keeler, J.; Hwang, T. L.; Shaka, A. J., EXCITATION SCULPTING IN HIGH-RESOLUTION NUCLEAR-MAGNETIC-RESONANCE SPECTROSCOPY - APPLICATION TO SELECTIVE NOE EXPERIMENTS. *Journal of the American Chemical Society* **1995,** *117* (14), 4199-4200.

62. Aguilar, J. A.; Nilsson, M.; Bodenhausen, G.; Morris, G. A., Spin echo NMR spectra without J modulation. *Chemical Communications* **2012,** *48* (6), 811-813.

63. Sklenar, V.; Piotto, M.; Leppik, R.; Saudek, V., GRADIENT-TAILORED WATER SUPPRESSION FOR H-1-N-15 HSQC EXPERIMENTS OPTIMIZED TO RETAIN FULL SENSITIVITY. *Journal of Magnetic Resonance Series A* **1993,** *102* (2), 241-245.

64. Sinnaeve, D., The Stejskal-Tanner equation generalized for any gradient shape-an overview of most pulse sequences measuring free diffusion. *Concepts in Magnetic Resonance Part A* **2012,** *40A* (2), 39-65.

65. Angulo, J.; Enríquez-Navas, P. M.; Nieto, P. M., Ligand–Receptor Binding Affinities from Saturation Transfer Difference (STD) NMR Spectroscopy: The Binding Isotherm of STD Initial Growth Rates. *Chemistry – A European Journal* **2010,** *16* (26), 7803-7812.

66. Quirós, M. T.; Angulo, J.; Muñoz, M. P., Kinetics of intramolecular chemical exchange by initial growth rates of spin saturation transfer difference experiments (SSTD NMR). *Chemical Communications* **2015,** *51* (50), 10222-10225.

67. Stimac, A.; Segota, S.; Sikiric, M. D.; Ribic, R.; Frkanec, L.; Svetlicic, V.; Tomic, S.; Vranesic, B.; Frkanec, R., Surface modified liposomes by mannosylated conjugates anchored via the adamantyl moiety in the lipid bilayer. *Biochimica Et Biophysica Acta-Biomembranes* **2012,** *1818* (9), 2252-2259.

68. Andersson, A.; Maler, L., Motilin-bicelle interactions: membrane position and translational diffusion. *FEBS letters* **2003,** *545* (2-3), 139-143.

69. Chou, J. J.; Baber, J. L.; Bax, A., Characterization of phospholipid mixed micelles by translational diffusion. *Journal of Biomolecular Nmr* **2004,** *29* (3), 299-308.

70. Andersson, A.; Maler, L., Magnetic resonance investigations of lipid motion in isotropic bicelles. *Langmuir* **2005,** *21* (17), 7702-7709.

71. Halassy Špoljar, B.; Čimbora, T.; Hanzl-Dujmović, I.; Dojnović, B.; Sabioncello, A.; Krstanović, M.; Tomašić, J., Influence of adjuvant-active peptidoglycan monomer on specific T cell responses in mice. *Vaccine* **2002,** *20* (29), 3543-3550.

72. Frkanec, R.; Travas, D.; Krstanovic, M.; Spoljar, B. H.; Ljevakovic, D.; Vranesic, B.; Frkanec, L.; Tomasic, J., Entrapment of peptidoglycans and adamantyltripeptides into liposomes: An HPLC assay for determination of encapsulation efficiency. *Journal of Liposome Research* **2003,** *13* (3-4), 279-294.

73. Over, B.; McCarren, P.; Artursson, P.; Foley, M.; Giordanetto, F.; Gronberg, G.; Hilgendorf, C.; Lee, M. D.; Matsson, P.; Muncipinto, G.; Pellisson, M.; Perry, M. W. D.; Svensson, R.; Duvall, J.

R.; Kihlberg, J., Impact of Stereospecific Intramolecular Hydrogen Bonding on Cell Permeability and Physicochemical Properties. *Journal of Medicinal Chemistry* **2014,** *57* (6), 2746-2754.

74. Wang, X.; Ramström, O.; Yan, M., Dynamic light scattering as an efficient tool to study glyconanoparticle-lectin interactions. *Analyst* **2011,** *136* (20), 4174-4178.

TOC graphics